Polymer Degradation and Stability 145 (2017) 60–69

Contents lists available at ScienceDirect

Polymer Degradation and Stability

journal homepage: www.elsevier.com/locate/polydegstab

Bionanocomposites based on PLA and halloysite nanotubes: From key properties to photooxidative degradation☆

Sandrine Therias [a], Marius Murariu [b, *], Philippe Dubois [b, c, **]

[a] Université Clermont Auvergne, CNRS, SIGMA Clermont, Institut de Chimie de Clermont-Ferrand, F-63000 Clermont–Ferrand, France
[b] Center of Innovation and Research in Materials and Polymers (CIRMAP), Laboratory of Polymeric and Composite Materials, University of Mons & Materia Nova Research Centre, Place du Parc 20, 7000 Mons, Belgium
[c] Luxembourg Institute of Science and Technology, Department Materials Research and Technology, L-4940 Hautcharage, Luxembourg

ARTICLE INFO

Article history:
Received 16 March 2017
Received in revised form
5 June 2017
Accepted 13 June 2017
Available online 15 June 2017

Keywords:
Biodegradable polyesters
Polylactide
Halloysite
Nanocomposites
Morphology
Mechanical properties
Degradation
UV irradiation
Photooxidation

ABSTRACT

Halloysite nanotubes (HNT) and polylactide (PLA) were dry-mixed and melt-compounded to produce PLA nanocomposites with up to 12 wt-% nanofiller. The key characteristics of PLA-HNT nanocomposites were evidenced as follows: good nanofiller distribution and dispersion assessed by transmission electron microscopy (TEM), high tensile strength (values above 60 MPa) and mechanical rigidity, with Young's modulus increasing with HNT loading. The impact resistance of PLA is not decreased, whereas as it was revealed under dynamic solicitation (DMA), addition of HNT led to the notable enhancement of storage modulus.

The degradation by photooxidation of PLA-HNT nanocomposites was compared to pristine PLA. The chemical modifications were evidenced by infrared (IR) and UV–visible spectroscopy, whereas from IR absorbance at 1845 cm^{-1} was determined the rate of degradation. Like in the case of other natural clays, HNT had a dramatic pro-degradant effect on the photooxidation of PLA, ascribed to the presence of chromophoric groups and/or iron impurities. Indeed, by comparing nanofillers of different purity, the photooxidation of PLA was found significantly reduced using HNT having about four times lower traces of iron.

The choice of HNT of adequate purity or/and its purification is looked as powerful method to reduce the photooxidative degradation of PLA nanocomposites.

1. Introduction

Poly(lactic acid) or polylactide (PLA), a biodegradable polyester produced from renewable resources, is used for various applications (biomedical, packaging, textile fibers and technical items) [1–7]. Currently, PLA has a leading position in the market of bio-based polymers and is undeniably regarded as one of the most promising sustainable alternatives to petroleum-based polymers. The high interest for PLA is mainly due to its interesting physico-mechanical properties, low carbon footprint, recycling possibility or biodegradability as option at the product end-of-life, broad possibilities of processing using traditional equipment [5,8,9]. Still, according to an excellent overview published by Andrzej Duda et al., aliphatic polyesters derived from lactides of various configurations (LL, DD and DL) are promising not only as materials for packaging and production of many other commonly used polymer products, but also for medical applications [10].

Regarding the application at larger scale, PLA is typically used to produce sustainable packaging materials and textile fibres, whereas recent trends and forecasts reveal that PLA is more and more considered for “durable” applications (automotive, electrical & electronic products, mechanical components, etc.), which require high performance materials. Accordingly, the addition of reinforcing fibers, micro- and/or nanofillers, and selected additives within PLA matrix, was considered as a powerful method allowing for obtaining specific end-use characteristics and major improvements of properties [3,11–15].

☆ Contribution in the frame of MoDeSt 2016 held in Krakow (Poland) and in the Memory of Professor Andrzej Duda, Polish Academy of Sciences, Lodz, Poland.

* Corresponding author.
** Corresponding author. Center of Innovation and Research in Materials and Polymers (CIRMAP), Laboratory of Polymeric and Composite Materials, University of Mons & Materia Nova Research Centre, Place du Parc 20, 7000 Mons, Belgium.
E-mail addresses: marius.murariu@materianova.be (M. Murariu), philippe.dubois@umons.ac.be (P. Dubois).

http://dx.doi.org/10.1016/j.polymdegradstab.2017.06.008
0141-3910/

Recently, halloysite nanotubes (HNT) [16–20] have been included between the nanofillers of interest for PLA [21–30]. In fact, as it comes out from the previous studies realized by us and other authors, due to several characteristic features such as nanoscale lumen, relatively high length-to-diameter ratio and low hydroxyl group density on their surface, HNT could be promising competitors and cheaper alternatives to widely investigated nanofillers such as CNT (carbon nanotubes) and OMLS (organo-modified layered silicates). As reported elsewhere, the chemical composition of HNT is like that of kaolinite, whereas considering the state of hydration, the ideal chemical formula can be expressed as $Al_2Si_2O_5(OH)_4$ x nH_2O (n equals 2 and 0 is representing respectively, the hydrated and dehydrated forms) [17,31]. Following HNT addition into PLA, several improvements were claimed, regarding especially the mechanical performances (tensile and flexural strength, rigidity, impact resistance, etc.) [21,32,33].

However, on one hand, some studies have been mainly devoted to the production and characterization of PLA-HNT nanocomposites with various nanofiller loadings, going even above 30 wt% [24], while on the other hand, only very limited information can be found connected to their ageing. Since these relatively new nanocomposites are potentially interesting for various applications (mechanical, automotive, packaging, others), it is important to overview and have more clear information about their performances, as well as, regarding their comportment during ageing under different conditions. The study of photochemical behavior of PLA-HNT nanocomposites is therefore of prime importance as the durability is the key factor for outdoor applications. Besides the hydrolytic degradation of PLA [34,35], the photochemical behavior of pristine PLA has already been described [36–39], and only few papers reported the effect of several fillers (particles of nano- or micro-size) on PLA photooxidation [40–43]. Clays such as OMLS have a pro-degradant effect on PLA oxidation [40,41]. On another side, a higher degradation was reported by adding micronized $CaSO_4$ particles to the PLA matrix [42], and with a photocatalytic filler such as ZnO [43], a higher oxidation of the PLA matrix was also observed, even though the UV-screening effect of the ZnO nanoparticles.

The aim of this work is to survey the key-properties of PLA-HNT nanocomposites produced by melt-compounding and to study their photooxidative degradation, while evidencing in a final experiment, the key-role played by the purity of nanofiller. The chemical modifications of PLA-HNT nanocomposites resulting from photooxidation were investigated by infrared (IR) and UV–visible spectroscopy. Influence of nanofiller loading on the mechanism of PLA oxidation was studied and the rates of degradation of PLA-HNT nanocomposites with HNT amount up to 12 wt% were compared to the pristine PLA. Finally, the study is a new attempt to include HNTs between the nanofillers of interest to produce bionanocomposites based on PLA, while evaluating their photooxidative degradation as determined by the loading and purity of nanofiller.

2. Experimental part

2.1. Materials

Poly(L,L-lactide) – hereafter called PLA, supplier NatureWorks LLC, was a grade designed for the extrusion of films (4032D) with M_n = 133 000, dispersity (D), M_w/M_n = 1.94 (M_w and M_n, being respectively, the weight- and number-average molar mass expressed in polystyrene equivalent), whereas according to the producer, other characteristics are as follows: D isomer content = 1.4%; relative viscosity = 3.94; residual monomer = 0.14%.

Halloysite nanotubes (HNT) were supplied by Aldrich with the following characteristics according to the technical sheet: nanotubes length = 1–3 μm (micrometer), surface area = 64 m^2 g^{-1}, pore volume = 1.26–1.34 mL g^{-1}. Following the Certificate of Analysis given by supplier for a first batch (hereinafter called lot 1), HNT contained about 14 900 ppm traces of metals (mainly iron (4700 ppm), calcium (5000 ppm), potassium (1500 ppm), sodium (1100 ppm), others). Additional own investigations have been performed by SEM and TEM [25], highlighting the existence of nanotubes of diverse length, ranging from hundreds of nanometers to above 2.5 μm, and typically characterized by outer tube diameter of 40–80 nm and lumen size of 10–30 nm. A milling process of surface treated/untreated HNT performed by the industrial producers was previously assumed [21,25]. HNT samples specifically used in this study have been further characterized by different techniques of analysis (e.g., TGA, SEM, TEM, EDX) and selected information will be used as support in the discussion of results. On the other hand, to validate the conclusion of degradation study in relation to the effects of HNT purity and iron content on the rate of PLA photooxidation, two different batches of natural halloysite containing different amount of iron have been compared (details in subsection 3.2.2.4).

2.2. Production of nanocomposites and preparation of samples

Before melt-blending, PLA was previously dried during 48 h at 60 °C using a recirculating air dryer, whereas the nanofiller (HNT) was dried during 48 h at 100 °C.

To produce nanocomposites, after a previous dry-mixing, the nanofiller was melt-compounded together with PLA at 200 °C under moderate shearing (cam blades) in a Brabender bench scale kneader (model 50 EHT) using a specific program (3 min premixing at 30 rpm, followed by 7 min mixing at 70 rpm). The premixing speed was fixed at 30 rpm to avoid an excessive increase of the torque during PLA melting. For the sake of comparison, the pristine PLA was processed by melt compounding under similar conditions. Table 1 shows the codification of PLA-based compositions selected for this study. Throughout this contribution, all percentages are given as weight percent (wt%).

To perform specimens for tensile and impact tests, plates of ~3 mm thickness were produced by compression molding at 190 °C by using an Agila PE20 hydraulic press. More specifically, the material was first pressed at low pressure for 200 s (3 degassing cycles), followed by a high-pressure cycle at 150 bars for 150 s. The resulting samples were then cooled under pressure (50 bars) for 300 s using water as cooling agent (temperature slightly higher than 10 °C). Specimens for tensile and Izod impact tests were obtained from plates by using a milling-machine (Ray-Ran CNC Milling Machine) in accordance with ASTM D 638-02a (specimens type V) and ASTM D 256-A norm (rectangular specimens of 60 × 13 × ~3 mm^3), respectively.

Films having a thickness of about 150 μm were used for the studies of degradation by photooxidation. The films were obtained by compression molding at 190 °C using the same compression

Table 1
The composition and codification of PLA based samples.

Entry	Sample code	Sample composition, wt.%	
		PLA	HNT
1	PLA	100	–
2	PLA3H	97	3
3	PLA6H	94	6
4	PLA9H	91	9
5	PLA12H	88	12

molding equipment. The polymer was firstly pressed at low pressure (10 bars) for 120s (2 degassing cycles at 50 and 100 bars), followed by a high-pressure cycle at 150 bars for 120s. This step was followed by quick cooling under pressure (50 bars) during 180s.

2.3. Characterization

2.3.1. Thermogravimetric analyses (TGA)

TGA were performed using a TGA Q50 (TA Instruments) with a heating ramp of 20 °C/min under air flow, from room temperature up to 600 °C (platinum pan, 60 cm^3/min air flow rate).

2.3.2. Differential scanning calorimetry (DSC)

DSC measurements were performed by using a DSC Q200 from TA Instruments under nitrogen flow. The procedure was as follows: first heating scan at 10 °C/min from 0 °C up to 200 °C, isotherms at this temperature for 2 min, then cooling down to −20 °C at 10 °C/min and finally, second heating scan from −20 °C to 200 °C at 10 °C/min. The first scan was realized to erase the anterior thermal history of the samples. The events of interest, i.e., the glass transition temperature (T_g), cold crystallization temperature (T_c), enthalpy of cold crystallization (ΔH_c), melting temperature (T_m) and melting enthalpy (ΔH_m), were determined from the second heating scan using the Universal Analysis 2000 software (TA Instruments). The degree of crystallinity (χc) was determined by subtracting ΔHc from ΔH_m, and by considering a melting enthalpy of 93 J/g for 100% crystalline PLA.

2.3.3. Mechanical testing

Tensile testing measurements were performed using a Lloyd LR 10K tensile bench in accordance to the ASTM D 638-02a norm at a speed rate of 1 mm/min with distance of 25.4 mm between grips. Notched impact strength (Izod) measurements were made by using a Ray-Ran 2500 pendulum impact tester and a Ray-Ran 1900 notching apparatus, in accordance to the ASTM D 256 norm (method A, 3.46 m/s impact speed, 0.668 kg hammer).

All mechanical tests were carried out by using specimens previously conditioned for at least 48 h at 20 ± 2 °C under a relative humidity of 50± 3% and the values were averaged out over five measurements.

2.3.4. Dynamic mechanical analysis (DMA)

DMA on selected samples (specimens of 60 × 12 × 2 mm^3 performed by injection molding at 200 °C, DSM micro-injection molding machine) were carried out using DMA 2980 apparatus (TA Instruments) in dual-cantilever bending mode. To avoid a different thermal history after the processing by injection molding or an additional crystallization process during testing, the specimens were annealed under similar conditions (at 110 °C under vacuum for 90 min). The dynamic storage and loss moduli (E′ and E″, respectively) were determined at a constant frequency of 1 Hz as a function of temperature from 0 to 140 °C, at a heating rate of 3 °C/min. For the sake of clarity, only one representative curve as the average of minimum two measurements was considered for each sample.

2.3.5. Transmission electron microscopy (TEM)

Transmission electron micrographs were obtained with a Philips CM200 apparatus using an accelerator voltage of 120 kV.

The nanocomposite samples (70–80 nm thick) were prepared with a Leica UCT ultracryomicrotome by cutting at −100 °C. Reported microphotographs represent typical morphologies as observed at, at least, three various places.

2.3.6. Irradiation of films and their characterization

The samples (films of 150 μm thickness) were irradiated under accelerated artificial conditions. The ageing device was a SEPAP 12/24 unit [44] from Atlas, which was equipped with four medium pressure mercury lamps (Novalamp RVC 400 W) located in a vertical position at each corner of the chamber. Wavelengths below 295 nm were filtered by the glass envelopes of the sources. The temperature at the surface of the samples was fixed at 60 °C.

- Infrared spectrometry: Infrared (IR) spectra were recorded in transmission mode using a Nicolet 760-FTIR spectrophotometer (nominal resolution of 4 cm^{-1}, 32 scans summations).
- UV–visible spectrometry: Changes in the UV–visible spectra were monitored with a Shimadzu UV-2101PC spectrophotometer equipped with an integrating sphere. The UV–visible spectra were recorded from 150 μm films in transmission mode.

3. Results and discussion

3.1. PLA-HNT nanocomposites: morphology and key-properties

3.1.1. Processing of PLA with HNT by melt-blending

Firstly, it is noteworthy reminding that PLA is very sensitive to temperature, shearing and hydrolysis, therefore it is stable in the molten state provided that it is adequately dried to reduce at minimum the water content (e.g. at less than 50 ppm) in the case of processing at high temperature [45]. Moreover, a significant reduction in melt viscosity ascribed to both, hydrolysis and to thermal degradation, was reported especially if PLA was not dried before testing [46]. Thus, it is of prime importance to dry PLA, but also it is a perquisite to dry/dehydrate the dispersed or reinforcing phases (such as HNT) added in the polyester matrix and processed by melt-compounding. Besides, HNT from different sources can vary in the level of hydration, morphology (dimension of inner and outer diameter, length, length-to-diameter ratio) and color, depending on the substitutional metals and on mineral origin [47], thus it is assumed that some of these factors can influence to some extent the properties of final PLA nanocomposites.

TGA of HNT (thermograms not shown here) revealed that during thermal heating the weight loss is seen in three distinct regions: **a**) a first weight loss up to around 100 °C, indicating the presence of absorbed free water (about 4 wt%); **b**) between 200 °C and 400 °C (d-TG shows a maximum at 280 °C), ascribed to the loss of water present between the layers of HNT. Nevertheless, this is corresponding to the formation of anhydrous HNT ($Al_2Si_2O_5(OH)_4$) with interlayer spacing of 7 Å which is traditionally named “halloysite 7 Å” [17,31]; **c)** dehydroxylation at higher temperature, with a maximum on d-TG curve at around 520 °C, the inorganic residue at the temperature of 600 °C being about 82%.

Interestingly as remark, the isothermal tests realized under air at 100 °C or 200 °C have shown that there is not a significant difference in the weight loss of HNT samples that can be linked to the drying under these conditions of temperature (loss of about 4% water).

To minimize PLA degradation by hydrolysis, the nanofiller must be carefully dried (see the experimental part). The specific surface treatments of HNT can reduce their sensitivity to water (re)absorption, whereas for some polymers requiring high-processing temperature (PC, PA, etc.) it is not totally excluded to use anhydrous halloysite ”7A”. (Nota Bene: for facility in the interpretation of results in the degradation study, in this work was preferred to use previously HNT dried, but without any additional surface treatment).

For instance, additional characterizations by size-exclusion chromatography (SEC) [48] have shown that there is not the

evidence of a significant decrease of molecular weights following the addition of HNT into PLA. Still, as a key-example, it is noteworthy mentioning that after melt-blending and processing by compression molding as films, neat PLA was characterized by a M_n (number-average molar mass expressed in polystyrene equivalent) of 87 300 (dispersity of 2.3), while at higher filling, i.e., by addition of 9% and 12% HNT, the M_n were respectively, 90 500 and 81 700 (dispersity of 2.2 and 2.3, respectively). Accordingly, using adequate experimental conditions, addition of HNT into PLA does not lead to the supplementary decreasing of molecular weights (the experimental errors for SEC measurements are estimated to be ±10%). On the other hand, it is believed that a forthcoming study regarding the modification of PLA molecular and thermo-mechanical parameters following both, the production of nanocomposites and photooxidation process, could lead to additional information of high interest.

3.1.2. Morphology study

Information regarding the morphology of nanofiller and of nanocomposites was mainly obtained through TEM analysis. Fig. 1 (**a**), (**b, c**) and (**d, e**), show respectively selected TEM pictures at different magnification of the nanofiller, and of nanocomposites produced by addition into PLA of 6% and 12% HNT. It is noticeable from the images recorded at lower magnification (Fig. 1b and d) that a good quality of the distribution of HNT is reached throughout PLA matrix, even using a nanofiller without any additional surface treatment (which is rather surprisingly) and by performing the melt-mixing under moderate shear (internal kneader). On the other hand, at higher loadings (i.e., 12% HNT), the presence of some aggregates (identified by black flashes in Fig. 1d) is occasionally evidenced in the TEM pictures. Following the TEM observations, HNTs appear well distributed and dispersed into PLA. As it is reported elsewhere, the limited intertubular contact area and rod-like geometry, the relatively weak tube–tube interactions due to few hydroxyl groups that are located on nanotube surface, can be considered between the factors that could explain their good distribution and dispersion [19,20].

3.1.3. Mechanical and thermo-mechanical properties

The reinforcing effect of HNT on different polymers (PLA is

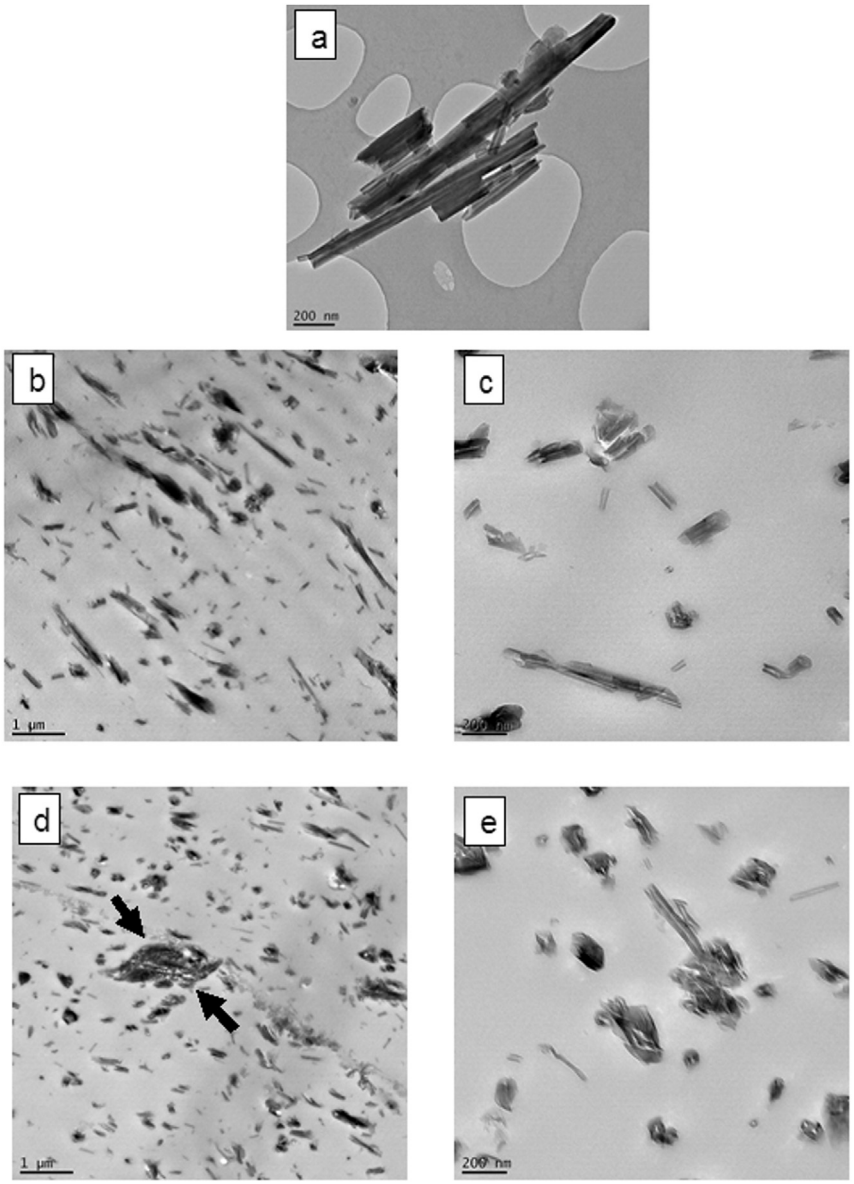

Fig. 1. (a–e). TEM pictures at different magnifications of HNT (**a**) of PLA-HNT nanocomposites containing 6% (**b** and **c**) and 12% (**d** and **e**) nanofiller.

included), frequently observed at low loadings, is generally ascribed to the rod-like and high aspect ratio structure, whereas the interfacial properties (nanotubes-polyester matrix) can play a key-role as well.

Fig. 2 shows the images of specimens used for tensile testing, while Fig. 3 displays the evolution of tensile strength and of rigidity (Young's modulus) in function of nanofiller loading. By comparison to neat PLA, the stress remains at similar values (maximum tensile strength above 60 MPa), but the rigidity is gradually increased in nanocomposites in quite good correlation with the amount of nanofiller. Further improvements in terms of tensile strength properties can be expected from the additional surface treatments of HNT [19,21], with beneficial contribution in the increase of interfacial interactions between nanotubes and the polyester matrix (PLA).

By comparison to other nanofillers (e.g. OMLS), which lead to PLA nanocomposites characterized by improved rigidity, mostly in the detriment of impact properties, the PLA-HNT nanocomposites do not show any decrease in impact resistance. In fact, for nanocomposites containing 3–12% HNT, the Izod impact resistance was found in the range 2.8–2.9 kJ/m^2, these values being even slightly better than those of neat PLA (2.7 kJ/m^2). This noteworthy behavior is commonly ascribed to the intrinsic stiffness of the nanotubes, dissipation of the impact energy via the nanotube bridging/pulling-out/breaking, and good nanofiller distribution throughout the polyester matrix [17].

The reinforcing effect of nanofiller was also evidenced following the testing under dynamic solicitations (DMA). Fig. 4**a** and **4b** show the temperature dependencies of storage (E′) and loss (E″) moduli of pristine PLA and of nanocomposites obtained by addition of up to 12% HNT. Addition of HNT led to the notable enhancement of storage modulus (E′). As an example, in correlation to nanofiller content E′ increases distinctly for nanocomposites, e.g., at 60 °C the value of E′ is 2240 MPa for neat PLA, 3150 MPa and 3870 MPa for PLA containing 6% and 12% HNT, respectively. However, at 12% HNT loading, the data reveal that there are not important differences between the temperatures corresponding to the maximum of E″ of neat PLA and those of nanocomposite (73.7 °C compared to 75.2 °C, respectively). The increase of E″ with the filler content is usually ascribed to the contribution of the mechanical loss generated at the interface regions between fillers and PLA matrix [49].

Additionally, based on the thermal characterizations (TGA and DSC, data summarized in Tables 2 and 3, respectively), it is noteworthy mentioning that addition of HNT into PLA lead to the slight decrease of $T_{5\%}$ (temperature for 5% weight loss, often considered as the initial decomposition temperature) and T_D (the temperature corresponding to the maximum rate of thermal degradation), whereas some improvements in the crystallization rate/degree was observed especially at higher HNT loading (i.e., at 12 wt%).

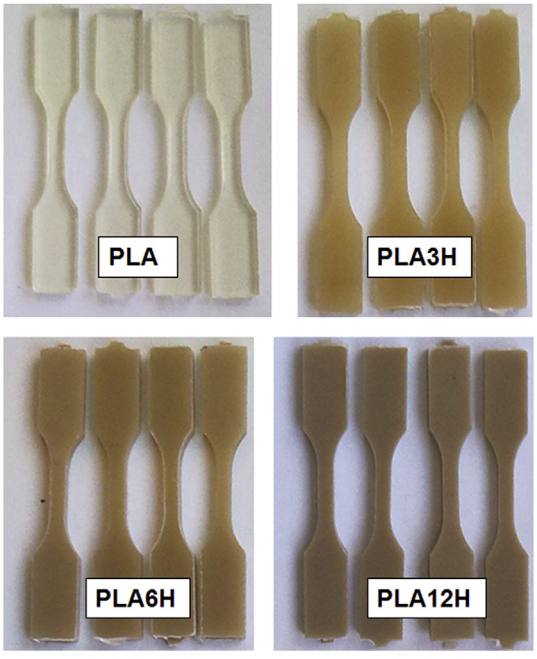

Fig. 2. Specimens of PLA and PLA-HNT nanocomposites used in tensile testing.

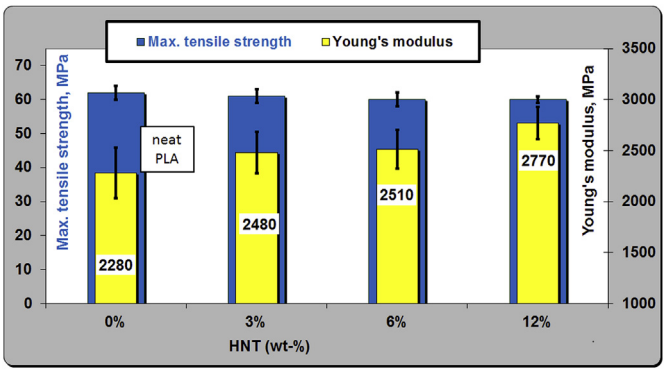

Fig. 3. Evolution of maximum tensile strength and Young's modulus of PLA and PLA–HNT nanocomposites with different loading of nanofiller.

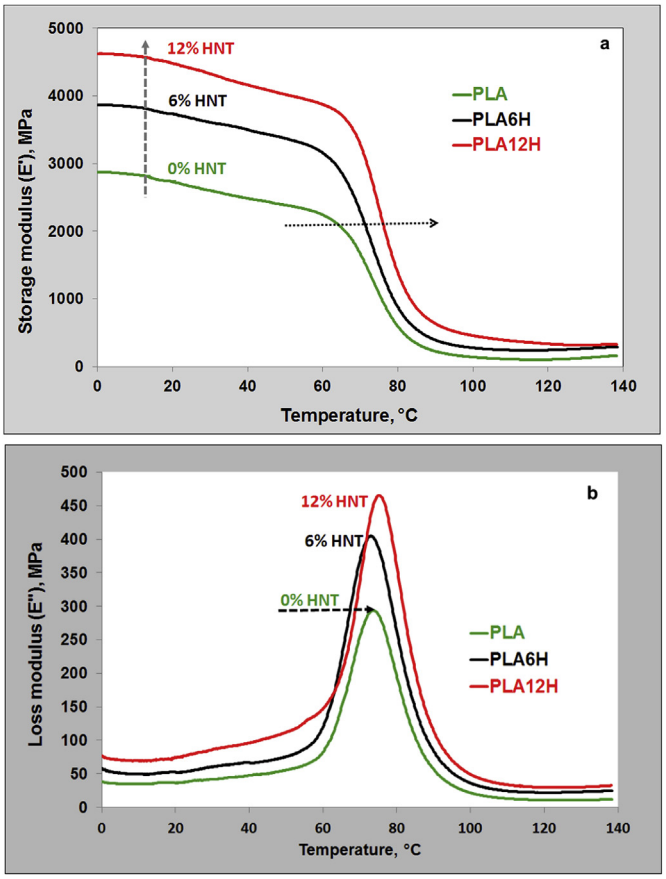

Fig. 4. (a, b). Dependencies of E' (**a**) and E" (**b**) vs. temperature: pristine PLA with respect to PLA-HNT nanocomposites.

Table 2
TGA data of pristine PLA and PLA-HNT nanocomposites (under air, 20 °C/min).

Entry	Sample	Temperature of 5% weight loss, °C	Temperature at max. rate of degradation, °C	Residue, %
1	PLA	329	377	0.3
2	PLA3H	320	376	2.8
3	PLA6H	319	373	5.2
4	PLA12H	316	370	10.1

Table 3
Comparative DSC data (second heating, 10 °C/min) of PLA and PLA-HNT nanocomposites.

Sample	T_g (°C)	T_c (°C)	ΔH_c (J g^{-1})	T_m (°C)	ΔH_m (J g^{-1})	χ_c, %
PLA	63	115	30.3	164.170	34.3	4.3
PLA3H	63	114	26.1	170	29.1	3.2
PLA6H	63	114	30.6	164.169	34.3	4.0
PLA12H	63	111	27.1	163.169	33.4	6.8

Finally, overall results suggest that, due to the specific features of the nanotubes and good HNT distribution/dispersion within polyester matrix, can be produced by melt-compounding nanocomposites showing good mechanical strength, rigidity and toughness, as key-properties.

3.2. Photooxidative degradation of PLA-HNT nanocomposites

3.2.1. IR and UV visible spectroscopy on films before irradiation

IR transmission spectra of PLA and PLA-HNT nanocomposites with increased content of HNT (from 3 to 12 wt%) are compared in Fig. 5.

The spectra show the characteristic absorption bands of PLA [42] and those resulting from the presence of HNT filler at 3695 cm^{-1}, 3620 cm^{-1}, 912 cm^{-1} and 535 cm^{-1} [24]. Moreover, the IR bands at 912 and 535 cm^{-1} are assigned respectively to the deformation of Al-O-Si and Al-OH groups [33]. Still, from the IR spectra it is assumed that the hydroxyl groups of PLA are interacting with HNT′ outer surface siloxane groups via hydrogen bonding [50], thus this could explain the good distribution of nanotubes and the mechanical performances of nanocomposites, even in the absence of nanofiller surface treatments.

The UV–visible spectra of the PLA and PLA-HNT nanocomposite films before irradiation are shown in Fig. 6. For all samples with HNT, an absorption band above 260 nm without any defined maximum is observed. This absorption can be attributed to the nanofiller as this effect increases with the amount of HNT in the nanocomposite film. One can also notice a light scattering effect due to the presence of HNT, which increases with the amount of the filler.

3.2.2. Photooxidation of PLA-HNT nanocomposites

3.2.2.1. Infrared analysis of irradiated films. The various PLA-HNT

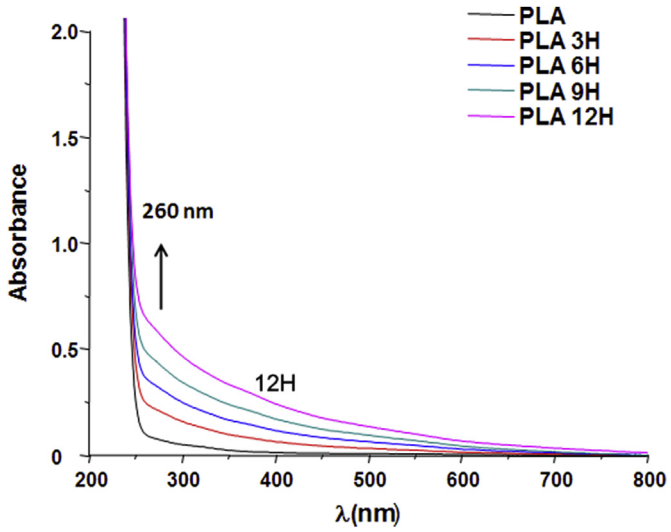

Fig. 6. UV–visible spectra of PLA and PLA-HNT nanocomposite films (3, 6, 9 and 12% HNT) before irradiation.

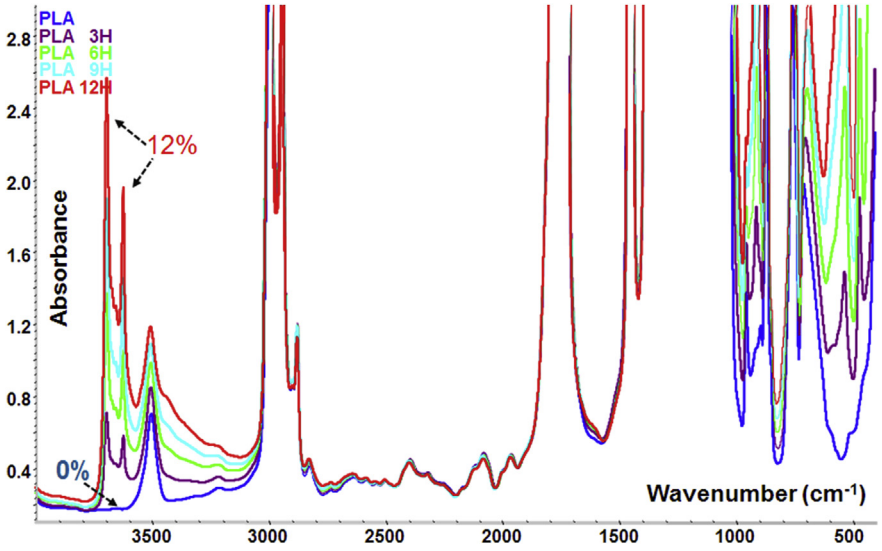

Fig. 5. IR spectra of PLA and PLA-HNT nanocomposite films (3, 6, 9 and 12% HNT) before irradiation.

nanocomposite films (from 3 to 12% HNT) were exposed to light in the presence of air and the chemical modifications resulting from photooxidation were monitored using IR spectroscopy. Fig. 7 **(a, b)** present the IR spectra of PLA3H films after irradiation.

The IR analysis of the PLA3H nanocomposite during photooxidation presents the formation of two absorption bands with maxima at 1845 cm^{-1} (clearly observed in the subtracted spectra in Fig. 7b) and at 3420 cm^{-1}, as previously observed and described for pristine PLA [42,43]. The IR band at 1845 cm^{-1} has been attributed to anhydride groups and the broad band in the hydroxyl domain to alcohol and carboxylic acid groups [43]. This indicates that the same PLA photooxidation products are formed in presence of HNT filler.

3.2.2.2. UV–visible analysis of irradiated films. UV–visible spectra of a PLA12H nanocomposite films (with 12% HNT) during photooxidation are presented in Fig. 8. The spectra show an increase of absorbance above 250 nm, corresponding to light scattering and yellowing (increase of absorbance at 400 nm). The films containing HNT filler become less and less transparent upon irradiation.

3.2.2.3. Rate of oxidation. To evaluate the influence of the amount of HNT on PLA photooxidation, the rate of PLA oxidation in the various PLA-HNT nanocomposite samples can be compared by

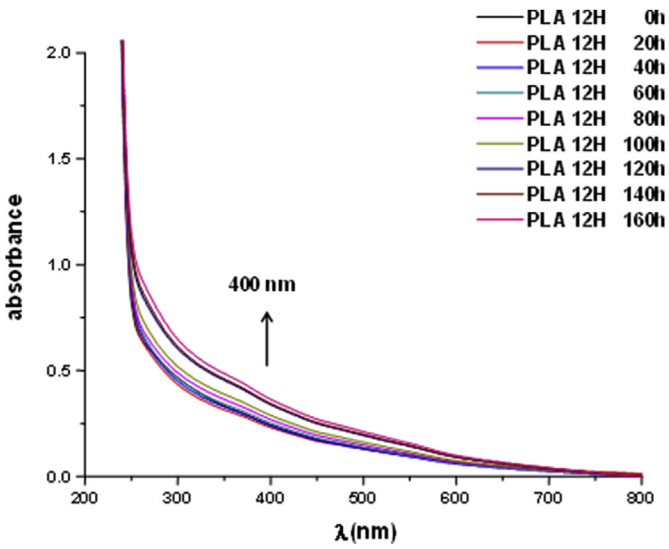

Fig. 8. UV–visible spectra of PLA12H nanocomposite films during photooxidation.

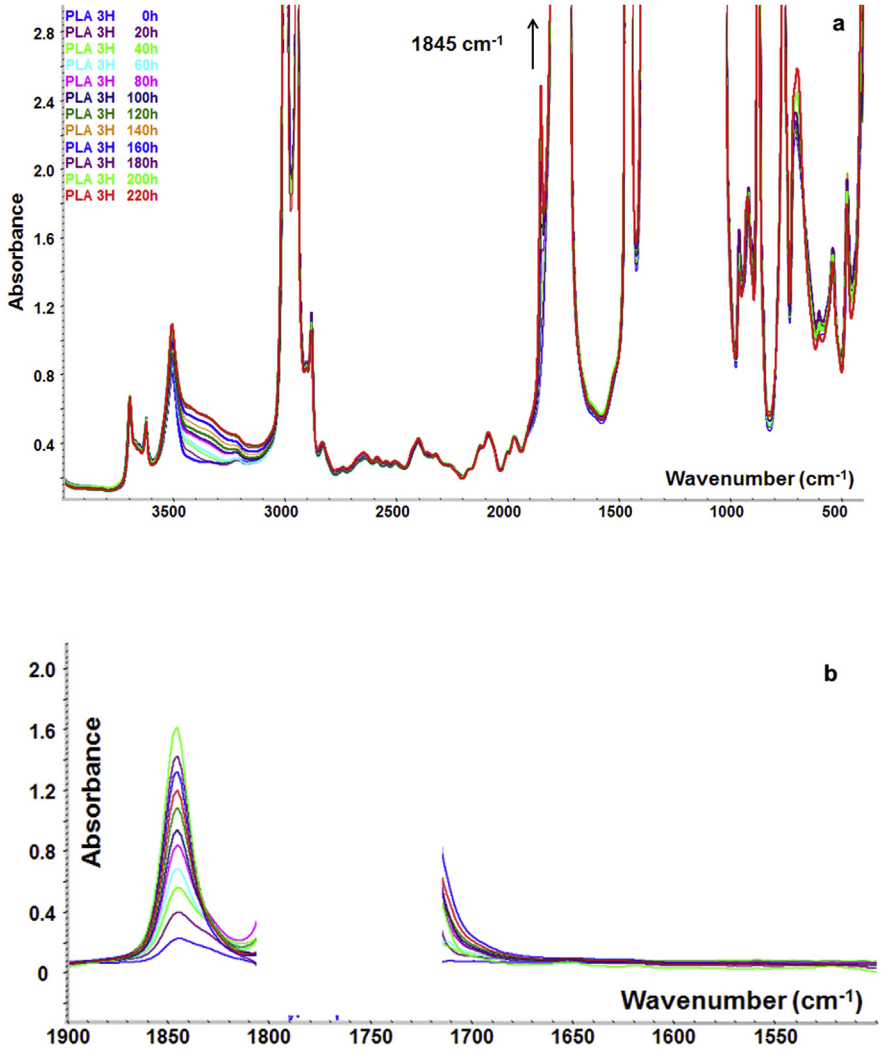

Fig. 7. (a, b). IR spectra of a PLA3H nanocomposite film during photooxidation: **a**) in the 4000-400 cm^{-1} domain; **b**) subtracted spectra in the carbonyl domain (1900-1500 cm^{-1}).

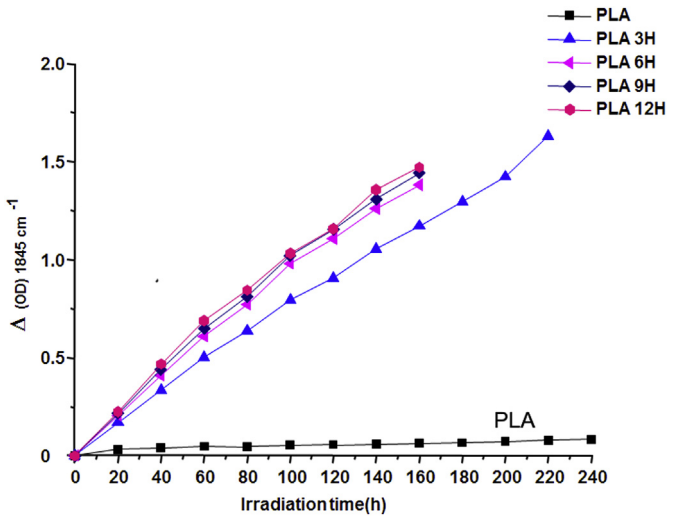

Fig. 9. Variation of absorbance at 1845 cm^{-1} as a function of irradiation time for PLA and PLA-HNT nanocomposite films (3, 6, 9 and 12% HNT).

plotting the increase of absorbance at 1845 cm^{-1} (measured in the subtracted IR spectra) with the irradiation time (Fig. 9).

The kinetic curves (Fig. 9) clearly indicate that the HNT filler has a pro-degradant effect on PLA photooxidation. Indeed, the rate of PLA oxidation is dramatically higher in presence of HNT compared to the neat PLA that shows very low levels of oxidation after 240 h of accelerated ageing. However, this effect ascribed to presence of HNT does not depend on the filler amount, as from 6 to 12% HNT the quantity of PLA oxidation products is the same in all the three nanocomposite films (PLA6H, PLA9H and PLA12H).

Undeniably, HNT has a pro-degradant effect on the photooxidation of PLA which can be attributed to the chromophoric impurities that can have an inducing effect on the radical oxidation mechanism of PLA, or the higher degradation of PLA-HNT nanocomposites can be due to the presence of iron impurities, as it was reported in the case of natural clays [51]. However, to explain these results, the chemical composition of HNT was supplementary analyzed by EDX (energy-dispersive X-ray spectroscopy). Oxygen, aluminum and silicon were the main elements detected (the weight percentages were respectively about 56.7%, 19.6% and 19.0%). Still, based on the same analysis, the nanofiller contained a small amount of carbon (1.3%), chlorine (0.8%), iron (0.5%), calcium, magnesium and some other elements in trace amount. Thus, the photooxidative degradation of PLA can be attributed to the presence of transition metal impurities such as iron, which can accelerate the oxidation of polymers by various processes including the decomposition of hydroperoxides [41,52], but other sources of degradation are not totally excluded. Although it is assumed that the photodegradation mechanism is the same as in PLA nanocomposites containing OMLS, which are shown to contribute to the increase of PLA degradation [41].

3.2.2.4. Effects of HNT purity and iron content on the rate of PLA photooxidation. To validate our hypothesis and to study the influence of impurities of iron on the PLA photooxidation rate, nanocomposites with 6 wt% of HNT (containing different amount of iron) were prepared and irradiated in the frame of additional investigations. Table 4 shows the quantification of trace metals determined by ICP spectrometry (Inductively Coupled Plasma) for two lots of HNT that have been compared in the frame of the degradation study. As remark, this information is obtained from the certificates of analysis given by supplier.

IR analysis was performed after irradiation and the rate of PLA photooxidation was plotted for the two different PLA6H in Fig. 10. For the nanocomposite samples with HNT (lot 2) particles containing about four times less traces of iron, the photooxidation rate of PLA is considerably reduced. This agrees with a relationship between iron content in HNT and the photodegradation of the polymer. Moreover, this result confirms the huge impact of iron impurity from nanofillers on the polymer oxidation. Based on these results, it comes out that to limit the photooxidative degradation it is of further interest to use designed stabilizers for the protection of PLA-HNT nanocomposites. On the other hand, the choice of nanofiller having adequate purity (i.e., less iron) or its purification when economically available, can pave the way to more performant products.

4. Conclusion

Halloysite nanotubes (HNT) are of interest as nanofillers to produce PLA nanocomposites using the melt-blending technology. The nanocomposites were characterized for highlighting the key-performances, whereas their degradation by photooxidation was compared to pristine PLA. Following the TEM observations, the nanofiller is easily dispersible into PLA matrix, while the thermal analyses (TGA, DSC) did not evidence any improvement in PLA stability (TGA) and significant modification of principal thermal parameters (DSC).

Interestingly, even using nanofiller without additional surface treatment, the mechanical properties were found as being very promising: high tensile strength and Young's modulus, whereas the impact resistance of PLA does not decrease. As demonstrated by DMA, melt-blending PLA with HNT leads to the enhancement of the storage modulus and this is looked as a possibility to use PLA in mechanical applications.

PLA-HNT nanocomposites as films were evaluated to obtain first information about their comportment during photooxidative degradation. The photochemical behavior of nanocomposites filled with 3–12% HNT clearly evidenced their advanced degradation by comparing to pristine PLA. Even at low amount of HNT (e.g., 3 wt %), IR spectra evidenced significant changes during degradation by presence of the band at 1845 cm^{-1} ascribed to the formation of anhydrides and which is well correlated to the degradation time. HNT has a pro-degradant effect on the photooxidation of PLA, process attributed to the presence chromophoric groups and/or to presence of traces of iron. The last hypothesis was confirmed by comparative testing of HNT with different amount of iron (4700 ppm versus 1200 ppm). The photooxidation rate of PLA was greatly reduced using HNT having about four times less traces of iron. Consequently, the co-addition of adequate stabilizers and

Table 4
Trace metal analysis (ICP) of HNT lots used in the degradation study.

HNT batch	Total metal traces (ppm)	Fe (ppm)	Ca (ppm)	Other elements in lower amount
HNT (lot 1)	15 000	4700	5000	K, Na, Mg, Mn …
HNT (lot 2)	4250	1200	1400	K, Mg, Zn, Na …

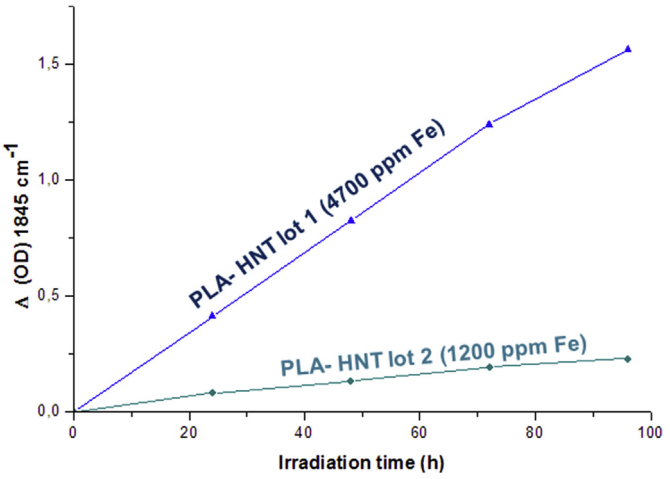

Fig. 10. Variation of absorbance at 1845 cm^{-1} as a function of irradiation time for PLA-6% HNT nanocomposite films containing nanofillers having different amount of iron: **a**) 4700 ppm Fe (lot 1); **b**) 1200 ppm Fe (lot 2).

utilization of nanofiller of higher purity will pave the way to the production of PLA-HNT nanocomposites with improved resistance to the photooxidative degradation.

Acknowledgements

Authors thank the Wallonia Region, Nord-Pas de Calais Region and European Commission for financial support in the frame of INTERREG IV: NANOLAC project (grant FW 1.1.8). They also thank their partners in the frame of NANOLAC project for helpful discussions. We are extremely grateful to Professor Andrzej Duda and Mirosław Pluta (Center of Molecular and Macromolecular Studies Lodz, Poland) for the scientific exchanges on the subject "PLA" and to the colleagues from Materia Nova (Belgium) for assistance in analyses. Authors particularly thank to Claire Poncet-Masson and David Bourgogne for technical support and assistance in the realization of irradiation experiments.

References

[1] R.E. Drumright, P.R. Gruber, D.E. Henton, Polylactic acid technology, Adv. Mater. 12 (23) (2000) 1841–1846, http://dx.doi.org/10.1002/1521-4095(200012)12, 23<1841::AID-ADMA1841>3.0.CO;2-E.
[2] A.P. Gupta, V. Kumar, New emerging trends in synthetic biodegradable polymers – polylactide: A critique, Eur. Polym. J. 43 (10) (2007) 4053–4074. http://dx.doi.org/10.1016/j.eurpolymj.2007.06.045.
[3] M. Murariu, P. Dubois, PLA composites: from production to properties, Adv. Drug Deliv. Rev. 107 (2016) 17–46. http://dx.doi.org/10.1016/j.addr.2016.04.003.
[4] R. Auras, B. Harte, S. Selke, An overview of polylactides as packaging materials, Macromol. Biosci. 4 (9) (2004) 835–864, http://dx.doi.org/10.1002/mabi.200400043.
[5] K. Hamad, M. Kaseem, H.W. Yang, F. Deri, Y.G. Ko, Properties and medical applications of polylactic acid: a review, Express Polym. Lett. 9 (5) (2015) 435–455, http://dx.doi.org/10.3144/expresspolymlett.2015.42.
[6] K.E. Perepelkin, Polylactide fibres: fabrication, properties, use, prospects. A review, Fibre Chem. 34 (2) (2002) 85–100, http://dx.doi.org/10.1023/a:1016359925976.
[7] B. Gupta, N. Revagade, J. Hilborn, Poly(lactic acid) fiber: an overview, Prog. Polym. Sci. 32 (4) (2007) 455–482. http://dx.doi.org/10.1016/j.progpolymsci.2007.01.005.
[8] X. Pang, X. Zhuang, Z. Tang, X. Chen, Polylactic acid (PLA): research, development and industrialization, Biotechnol. J. 5 (11) (2010) 1125–1136, http://dx.doi.org/10.1002/biot.201000135.
[9] E.T.H. Vink, K.R. Rábago, D.A. Glassner, B. Springs, R.P. O'Connor, J. Kolstad, P.R. Gruber, The sustainability of NatureWorks™ polylactide polymers and Ingeo™ polylactide fibers: an update of the future, Macromol. Biosci. 4 (6) (2004) 551–564, http://dx.doi.org/10.1002/mabi.200400023.
[10] S. Slomkowski, S. Penczek, A. Duda, Polylactides—an overview, Polym. Adv. Technol. 25 (5) (2014) 436–447, http://dx.doi.org/10.1002/pat.3281.
[11] J.-M. Raquez, Y. Habibi, M. Murariu, P. Dubois, Polylactide (PLA)-based nanocomposites, Prog. Polym. Sci. 38 (10–11) (2013) 1504–1542. http://dx.doi.org/10.1016/j.progpolymsci.2013.05.014.
[12] R.M. Rasal, A.V. Janorkar, D.E. Hirt, Poly(lactic acid) modifications, Prog. Polym. Sci. 35 (3) (2010) 338–356. http://dx.doi.org/10.1016/j.progpolymsci.2009.12.003.
[13] M. Murariu, F. Laoutid, P. Dubois, G. Fontaine, S. Bourbigot, E. Devaux, C. Campagne, M. Ferreira, S. Solarski, Chapter 21-Pathways to Biodegradable Flame Retardant Polymer (Nano)Composites, Polymer Green Flame Retardants, Elsevier, Amsterdam, 2014, pp. 709–773. http://dx.doi.org/10.1016/B978-0-444-53808-6.00021-4.
[14] T. Mukherjee, N. Kao, PLA based biopolymer reinforced with natural fibre: a review, J. Polym. Environ. 19 (3) (2011) 714–725, http://dx.doi.org/10.1007/s10924-011-0320-6.
[15] M. Jamshidian, E.A. Tehrany, M. Imran, M. Jacquot, S. Desobry, Poly-lactic acid: production, applications, nanocomposites, and release studies, Compr. Rev. Food Sci. Food Saf. 9 (5) (2010) 552–571, http://dx.doi.org/10.1111/j.1541-4337.2010.00126.x.
[16] E. Joussein, S. Petit, J. Churchman, B. Theng, D. Righi, B. Delvaux, Halloysite clay minerals - a review, Clay Miner. 40 (4) (2005) 383–426, http://dx.doi.org/10.1180/0009855054040180.
[17] P. Yuan, D. Tan, F. Annabi-Bergaya, Properties and applications of halloysite nanotubes: recent research advances and future prospects, Appl. Clay Sci. 112–113 (2015) 75–93. http://dx.doi.org/10.1016/j.clay.2015.05.001.
[18] D. Rawtani, Y.K. Agrawal, Multifarious applications of halloysite nanotubes: a review, Rev. Adv. Mater. Sci. 30 (3) (2012) 282–295.
[19] M. Liu, Z. Jia, D. Jia, C. Zhou, Recent advance in research on halloysite nanotubes-polymer nanocomposite, Prog. Polym. Sci. 39 (8) (2014) 1498–1525. http://dx.doi.org/10.1016/j.progpolymsci.2014.04.004.
[20] M. Du, B. Guo, D. Jia, Newly emerging applications of halloysite nanotubes: a review, Polym. Int. 59 (5) (2010) 574–582, http://dx.doi.org/10.1002/pi.2754.
[21] M. Murariu, A.-L. Dechief, Y. Paint, S. Peeterbroeck, L. Bonnaud, P. Dubois, Polylactide (PLA)—halloysite nanocomposites: production, morphology and key-properties, J. Polym. Environ. 20 (4) (2012) 932–943, http://dx.doi.org/10.1007/s10924-012-0488-4.
[22] G. Gorrasi, R. Pantani, M. Murariu, P. Dubois, PLA/Halloysite nanocomposite films: water vapor barrier properties and specific key characteristics, Macromol. Mater. Eng. 299 (1) (2014) 104–115, http://dx.doi.org/10.1002/mame.201200424.
[23] S.H.K.Y.H. Kim, H.J. Choi, K. Choi, N. Kao, S.N. Bhattacharya, R.K. Gupta, Thermal, mechanical, and rheological characterization of polylactic acid/halloysite nanotube nanocomposites, J. Macromol. Sci. Part B 55 (7) (2016) 680–692, http://dx.doi.org/10.1080/00222348.2016.1187054.
[24] M. Liu, Y. Zhang, C. Zhou, Nanocomposites of halloysite and polylactide, Appl. Clay Sci. 75–76 (2013) 52–59. http://dx.doi.org/10.1016/j.clay.2013.02.019.
[25] D. Notta-Cuvier, M. Murariu, J. Odent, R. Delille, A. Bouzouita, J.-M. Raquez, F. Lauro, P. Dubois, Tailoring polylactide properties for automotive applications: effects of Co-Addition of halloysite nanotubes and selected plasticizer, Macromol. Mater. Eng. 300 (7) (2015) 684–698, http://dx.doi.org/10.1002/mame.201500032.
[26] K. Prashantha, B. Lecouvet, M. Sclavons, M.F. Lacrampe, P. Krawczak, Poly(-lactic acid)/halloysite nanotubes nanocomposites: structure, thermal, and mechanical properties as a function of halloysite treatment, J. Appl. Polym. Sci. 128 (3) (2013) 1895–1903, http://dx.doi.org/10.1002/app.38358.
[27] B.J. Rashmi, K. Prashantha, M.F. Lacrampe, P. Krawczak, Toughening of poly(Lactic acid) without sacrificing stiffness and strength by melt-blending with polyamide 11 and selective localization of halloysite nanotubes, Express Polym. Lett. 9 (8) (2015) 721–735, http://dx.doi.org/10.3144/expresspolymlett.2015.67.
[28] W. Wu, X. Cao, Y. Zhang, G. He, Polylactide/halloysite nanotube nanocomposites: thermal, mechanical properties, and foam processing, J. Appl. Polym. Sci. 130 (1) (2013) 443–452, http://dx.doi.org/10.1002/app.39179.
[29] R.T. De Silva, M. Soheilmoghaddam, K.L. Goh, M.U. Wahit, S.A.H. Bee, S.-P. Chai, P. Pasbakhsh, Influence of the processing methods on the properties of poly(lactic acid)/halloysite nanocomposites, Polym. Compos. 37 (3) (2016) 861–869, http://dx.doi.org/10.1002/pc.23244.
[30] C. Kaynak, I. Kaygusuz, Consequences of accelerated weathering in polylactide nanocomposites reinforced with halloysite nanotubes, J. Compos. Mater. 50 (3) (2016) 365–375, http://dx.doi.org/10.1177/0021998315575038.
[31] Y. Zhang, A. Tang, H. Yang, J. Ouyang, Applications and interfaces of halloysite nanocomposites, Appl. Clay Sci. 119 (Part 1) (2016) 8–17. http://dx.doi.org/10.1016/j.clay.2015.06.034.
[32] M. Murariu, A.-L. Dechief, R. Ramy-Ratiarison, Y. Paint, J.-M. Raquez, P. Dubois, Recent advances in production of poly(lactic acid) (PLA) nanocomposites: a versatile method to tune crystallization properties of PLA, Nanocomposites 1 (2) (2015) 71–82, http://dx.doi.org/10.1179/2055033214Y.0000000008.
[33] J. Guo, J. Qiao, X. Zhang, Effect of an alkalized-modified halloysite on PLA crystallization, morphology, mechanical, and thermal properties of PLA/halloysite nanocomposites, n/a-n/a, J. Appl. Polym. Sci. (2016), http://dx.doi.org/10.1002/app.44272.
[34] K. Odelius, A. Höglund, S. Kumar, M. Hakkarainen, A.K. Ghosh, N. Bhatnagar, A.-C. Albertsson, Porosity and pore size regulate the degradation product profile of polylactide, Biomacromolecules 12 (4) (2011) 1250–1258, http://dx.doi.org/10.1021/bm1015464.
[35] H. Tsuji, T. Saeki, T. Tsukegi, H. Daimon, K. Fujie, Comparative study on

hydrolytic degradation and monomer recovery of poly(l-lactic acid) in the solid and in the melt, Polym. Degrad. Stab. 93 (10) (2008) 1956–1963. http://dx.doi.org/10.1016/j.polymdegradstab.2008.06.009.
[36] E. Ikada, Photo- and bio-degradable polyesters. Photodegradation behaviors of aliphatic polyesters, J. Photopolym. Sci. Technol. 10 (2) (1997) 265–270, http://dx.doi.org/10.2494/photopolymer.10.265.
[37] H. Tsuji, Y. Echizen, Y. Nishimura, Photodegradation of biodegradable polyesters: a comprehensive study on poly(l-lactide) and poly(ε-caprolactone), Polym. Degrad. Stab. 91 (5) (2006) 1128–1137. http://dx.doi.org/10.1016/j.polymdegradstab.2005.07.007.
[38] A. Copinet, C. Bertrand, S. Govindin, V. Coma, Y. Couturier, Effects of ultraviolet light (315 nm), temperature and relative humidity on the degradation of polylactic acid plastic films, Chemosphere 55 (5) (2004) 763–773. http://dx.doi.org/10.1016/j.chemosphere.2003.11.038.
[39] H. Tsuji, Y. Echizen, Y. Nishimura, Enzymatic degradation of poly(l-lactic acid): effects of UV irradiation, J. Polym. Environ. 14 (3) (2006) 239–248, http://dx.doi.org/10.1007/s10924-006-0023-6.
[40] L. Zaidi, M. Kaci, S. Bruzaud, A. Bourmaud, Y. Grohens, Effect of natural weather on the structure and properties of polylactide/Cloisite 30B nanocomposites, Polym. Degrad. Stab. 95 (9) (2010) 1751–1758. http://dx.doi.org/10.1016/j.polymdegradstab.2010.05.014.
[41] S. Bocchini, K. Fukushima, A.D. Blasio, A. Fina, A. Frache, F. Geobaldo, Polylactic acid and polylactic acid-based nanocomposite photooxidation, Biomacromolecules 11 (11) (2010) 2919–2926, http://dx.doi.org/10.1021/bm1006773.
[42] M. Gardette, S. Thérias, J.-L. Gardette, M. Murariu, P. Dubois, Photooxidation of polylactide/calcium sulphate composites, Polym. Degrad. Stab. 96 (4) (2011) 616–623. http://dx.doi.org/10.1016/j.polymdegradstab.2010.12.023.
[43] S. Therias, J.-F. Larché, P.-O. Bussière, J.-L. Gardette, M. Murariu, P. Dubois, Photochemical behavior of polylactide/ZnO nanocomposite films, Biomacromolecules 13 (10) (2012) 3283–3291, http://dx.doi.org/10.1021/bm301071w.
[44] J.-L. Philippart, C. Sinturel, J.-L. Gardette, Influence of light intensity on the photooxidation of polypropylene, Polym. Degrad. Stab. 58 (3) (1997) 261–268. http://dx.doi.org/10.1016/S0141-3910(97)00056-6.
[45] L.T. Lim, R. Auras, M. Rubino, Processing technologies for poly(lactic acid), Prog. Polym. Sci. 33 (8) (2008) 820–852. http://dx.doi.org/10.1016/j.progpolymsci.2008.05.004.
[46] V. Speranza, A. De Meo, R. Pantani, Thermal and hydrolytic degradation kinetics of PLA in the molten state, Polym. Degrad. Stab. 100 (2014) 37–41. https://doi.org/10.1016/j.polymdegradstab.2013.12.031.
[47] K.-M. Ng, Y.-T.R. Lau, C.-M. Chan, L.-T. Weng, J. Wu, Surface studies of halloysite nanotubes by XPS and ToF-SIMS, Surf. Interface Analysis 43 (4) (2011) 795–802, http://dx.doi.org/10.1002/sia.3627.
[48] M. Murariu, Y. Paint, O. Murariu, J.-M. Raquez, L. Bonnaud, P. Dubois, Current progress in the production of PLA–ZnO nanocomposites: beneficial effects of chain extender addition on key properties, J. Appl. Polym. Sci. 132 (48) (2015), http://dx.doi.org/10.1002/app.42480 n/a-n/a.
[49] M. Pluta, M. Murariu, M. Alexandre, A. Galeski, P. Dubois, Polylactide compositions. The influence of ageing on the structure, thermal and viscoelastic properties of PLA/calcium sulfate composites, Polym. Degrad. Stab. 93 (5) (2008) 925–931. http://dx.doi.org/10.1016/j.polymdegradstab.2008.02.001.
[50] R.T. De Silva, P. Pasbakhsh, K.L. Goh, S.P. Chai, J. Chen, Synthesis and characterisation of poly (lactic acid)/halloysite bionanocomposite films, J. Compos. Mater. 48 (30) (2013) 3705–3717, http://dx.doi.org/10.1177/0021998313513046.
[51] S. Morlat, B. Mailhot, D. Gonzalez, J.-L. Gardette, Photo-oxidation of polypropylene/montmorillonite nanocomposites. 1. Influence of nanoclay and compatibilizing agent, Chem. Mater. 16 (3) (2004) 377–383, http://dx.doi.org/10.1021/cm031079k.
[52] S. Bocchini, A. Frache, Comparative study of filler influence on polylactide photooxidation, Express Polym. Lett. 7 (5) (2013) 431–442, http://dx.doi.org/10.3144/expresspolymlett.2013.40.